The Potential of Higher Eigenmodes in Magnetic Resonance Force Microscopy

Rembrandt Donkersloot

May 2016

The Potential of Higher Eigenmodes in Magnetic Resonance Force Microscopy

Master Thesis

Submitted in partial fulfilment of the
requirements for the degree of
Master of Science
in
Physics

Author:
Rembrandt Donkersloot

Kamerlingh Onnes Laboratory, Leiden
Leiden University, The Netherlands, May 2016

Mentor: J.J.T. Wagenaar, MSc.
Supervisor and First Corrector: prof. dr. ir. T.H. Oosterkamp
Second Corrector: dr. M. Allan

Contents

Abstract

An indispensable ingredient for nanoscale imaging within the field of Magnetic Resonance Force Microscopy (MRFM) is a radiofrequency (RF) source. Conventional RF-sources constitute a significant impediment for MRFM experiments at extreme low temperatures and consequently form a major obstacle towards the single-spin measurement. In this thesis we have introduced a non-trivial method where an intrinsic property of an MRFM force sensor is exploited for the generation of an ultra-low dissipative RF-field. Using MRFM as a probe for local nuclear magnetic resonance (NMR) experiments on copper nuclei at millikelvin temperatures, we have demonstrated that the correct implementation of this feature resulted in an amplification of the NMR signal by more than a factor 2. Based on these findings, we propose an adjusted design of the force sensor that could contribute towards a significantly improved imaging sensitivity as established in MRFM experiments to date.

Chapter 1

Introduction

Motivated by the urge for a tool that allows non-destructive imaging of biological tissue in 3 spatial dimensions at atomic resolution, Sidles proposed in 1991 to combine the principles behind Magnetic Force Microscopy (MFM) and Magnetic Resonance Imaging (MRI) into a new field of force microscopy: Magnetic Resonance Force Microscopy (MRFM) or nano-MRI [1, 2]. The technique is based on a force interaction measurement between an extremely sensitive force sensor and the net magnetic moment of a spin ensemble under study. Similar to MRI, magnetic field gradients are used for the selection of spins such that, in principle, individual nuclei can be manipulated and detected. However, the interaction force between a nucleus and a typical MRFM force sensor is of the order of zepto[1] Netwon, making single nuclei extremely difficult to detect. Yet, the state of the art MRFM has shown its potential after achieving to detect a single electron spin [3]. Even more impressive, researchers at the IBM Research Division managed to 3D-image a Tobacco Mosaic Virus with a 5 nanometer resolution, corresponding to a sensitivity of 100 protons[4].

1.1 Basic principles of MRFM

The force sensor of a conventional MRFM set-up consists of a ferromagnetic particle attached at an ultra-soft cantilever. The net nuclear magnetic moment $\boldsymbol{\mu}$ of a sample under study interact with the external static magnetic field $\boldsymbol{B}$ of the magnetic particle: $E = \boldsymbol{\mu} \cdot \boldsymbol{B}$. The external field is conventionally aligned in the $\hat{\mathbf{z}}$ direction, $\boldsymbol{B} = B_0\hat{\mathbf{z}}$. Due to the Zeeman-effect, the nuclei energy levels will split into $2s+1$ energy levels with energy $\hbar m_i \gamma B_0$, where s and $m_i = \{-s, -s+1, ..., s-1, s\}$ are the spin and magnetic quantum number respectively, γ is the gyromagnetic ratio, and $\hbar$ is the reduced Planck constant.

For a spin-1/2 particle ($s = 1/2$) in an external magnetic field, one can easily show that the expectation value of its magnetic moment will precesses around the applied static

[1] zepto: 10^{-21}

field, rotating clockwise or rotating anti-clockwise. The precession frequency is defined as the Larmor frequency ω_L and is proportional with the amplitude of the static field, $\omega_L = \gamma B_0$. Thus, the spin can take either a state in which the magnetic moment is aligned or anti-aligned with $\boldsymbol{B}$, corresponding to the so-called 'up' or 'down' state with energy $E_{up} = -\frac{\hbar}{2}\gamma B_0$ and $E_{down} = +\frac{\hbar}{2}\gamma B_0$ respectively.

The energy levels of a spin can be coupled when introducing a time-dependent perturbation, such as RF-radiation with RF-frequency $\Omega = \gamma B_1$, where B_1 is the magnetic field strength of the oscillating radiation. In the case the energy of this periodic perturbation $E_{pert} = \hbar\Omega$ matches with the spacing of the spin's energy levels, $\Delta E = \hbar\gamma B_0$, the eigenstates will completely reverse periodically over time, a phenomenon which is known as Rabi-oscillations. Since $\hbar\Omega = \hbar\gamma B_0$, the condition for Rabi-oscillations to occur is $\Omega = \omega_L$. For reasons that will become clear in a moment, this condition is called the 'resonance condition'.

More general, for arbitrary Ω, the spin states will evolve with time t according to:

$$P_{down} = \frac{\Omega^2}{\Omega_R^2}\sin\left(\frac{\Omega_R t}{2}\right) \tag{1.1}$$

$$P_{down} = \frac{\Delta^2}{\Omega_R^2} + \frac{\Omega^2}{\Omega_R^2}\cos\left(\frac{\Omega_R t}{2}\right) \tag{1.2}$$

Here, Δ is the offset in applied RF-frequency, $\Delta \equiv |\omega_L - \Omega|$, and $\Omega_R^2 \equiv \Omega^2 + \Delta^2$ is defined as *the total Rabi frequency*.

Now, for a spin ensemble in thermal equilibrium with the environment (referred to as 'the lattice') at temperature T, there is a small surplus of spins in the lowest energy state, as given by the Boltzmann factor $\exp\{\mu B m_i / s \mathrm{k_B} T\}$, which results in an average net magnetic moment $\langle\mu_0\rangle$ in the direction of $\boldsymbol{B}$. Here, $\mathrm{k_B}$ is the Boltzmann constant. When applying radiation that fulfils the resonance condition, the spin ensemble will absorb energy. Due to the induced transitions, the initial spin population difference will eventually (almost) disappear, and the spin populations are said to be 'saturated': It can be shown that for a certain minimal radiation time combined with a sufficiently large B_1-field strength, the initial net magnetization will decrease to a saturation value of $\langle\mu_0\rangle \cdot (1+s)^{-1}$, where s is the saturation parameter, $s = \gamma^2 B_1^2 T_1^2 T_2^2$. Here T_1 and T_2 are known as the spin-lattice and the spin-spin relaxation times, and are a measure for the interaction of a single spin with the lattice and with neighbouring spins respectively.

More specifically, our working definition of the spin-spin relaxation time is equal to the T_2-time F. Bloch introduced in 1952 [5]:

$$\frac{1}{T_2} = \gamma B_{loc} \approx \frac{\gamma^2 \hbar}{r^3} \tag{1.3}$$

Here, $B_{loc} \approx \sum_{NN} B_{dd}$ is the additional field a single spin experiences due to the magnetic moments of its nearest neighbours (NN) at distance r.

Moreover, within an MRFM experiment, the net net magnetic moment of a spin ensemble under study exerts a force $F = \nabla E$ on the cantilever, resulting in a shift in the cantilevers stiffness: $k_{spin} = \mu \frac{\mathrm{d}^2 B_0}{\mathrm{d}z^2}$. Consequently, the natural resonance frequency of the cantilever f_0 will shift, $f_0 \rightarrow \tilde{f}_0 = f_0 + \Delta f$, and serves as a measure for the cantilever-nuclei interaction[2]. When applying an RF-pulse, spins precessing at a Larmor frequency $\omega_L = \Omega$ will obey the resonance condition. Since the B_0-source (the magnetic particle) is not uniform, only a small fraction of the spins will be at resonance. For a spherical magnetic particle, which can be modelled as a simple dipole with magnetic moment $\boldsymbol{\mu}$, the collection of spins at resonance forms a spherical slice in the sample under study, which we define as the *resonance slice*. The pulse will saturate the spin populations in the resonance slice and the interaction between the spin sample and the cantilever will be reduced. After the pulse, the cantilever's resonance frequency will restore to $\tilde{f}_0$ with a single exponential, characterised by T_1:

$$\Delta f(t) = f_0 + \Delta f(0) \cdot e^{-t/T_1} \tag{1.4}$$

Furthermore, the sensitivity $\Delta\mu$ of a typical MRFM experiment is related to the frequency shift:

$$\Delta\mu = \frac{1}{|\nabla B_0|} \sqrt{4 \mathrm{k_B} T \Gamma \Delta f} \tag{1.5}$$

and is therefore mainly limited by thermal noise and the cantilever properties which determine the friction of the cantilever and the magnetic field gradient ∇B_0. We thus notice that MRFM experiments require magnetic particles with a strong field gradient [7]. Concerning the further improvement of the sensitivity within MRFM, the strategy of the nano-MRI group at Leiden University is to work at ultra low temperatures. In order to achieve this, several technical challenges need to be conquered. For instance, in conventional MRFM, frequency shifts are measured by analysing the cantilever dynamics using a laser interferometer read-out. However, combined with the dissipation generated by the RF-source,

[2] A recent analysis shows a more complete picture of the interaction between a magnetic spin and a force sensor, taking into account the motion of the cantilever and the interaction of the spin with its neighbouring spins and the lattice [6].

the laser will heat up the cantilever and sample such that MRFM at temperatures below 300 mK are not possible. Alternatively, we use a Superconducting Quantum Interferometer Device (SQUID) to determine the cantilever's motion, which enables MRFM measurements at millikelvin temperatures [8].

1.2 This thesis

In this thesis, we will study the spin system of a copper sample at millikelvin temperatures. More specifically, we will study the relaxation behaviour of the copper nuclei spins and we will try to measure a frequency shift as function of RF-pulse frequency, width and amplitude. By doing so, we will look for those measurement settings that correspond to a maximum frequency shift. We will see that the higher modes of the force sensor play an important role in the final outcomes. Using equation 1.5, we can extract the T_1 time of copper [3], which should be equal to the T_1 time as stated by the Korringa relation for copper [9]:

$$T_1 T = 1.1\,\mathrm{sK} \tag{1.6}$$

Measuring relaxation times is a common practise in Nuclear Magnetic Resonance (NMR). Therefore, we will refer to the frequency measurements as 'NMR-measurements'.

[3] We study a sample containing the isotopes Cu-63 and Cu-65, with natural abundance 69% and 31%

Chapter 2

Material and Methods

In this chapter we will provide a basic description of the experimental set-up and measurement characterization. A very detailed description of the full experimental instrumentation as well as the sample under study can be found in the PhD theses of Wijts [10] and Den Haan [11] respectively. However, the reader may use this chapter as a guide to understand the experimental foundation of the main results as reported in chapter 3, without the need for additional reference searches.

2.1 Brief overview of the experimental set-up

Figure 2.1a shows the heart of our MRFM set-up, which consists of 3 major elements: a sample containing spins, a force sensor, and a spin manipulation/detection circuit. This thesis is devoted to experiments on copper. We used a commercial cryogen-free dilution refrigerator [1] with the implementation of vibration-reducing modifications, which allowed us to perform all experiments at millikelvin temperatures.

The force sensor consists of an ultra soft single crystalline silicon cantilever that are fabricated by Chui et al. [12], with dimensions length: 145 μm, depth: 5 μm and height: 0.1 μm. A spherical NdFeB[2] ferromagnetic particle with diameter: 3.43 μm is attached at the tip of the cantilever. An integrated positioning system allows us to align the cantilever in 3 dimensions with respect to the detection chip (containing the sample and detection/manipulation circuit) within a range of 1 mm and up to 1 μm precission.

The loaded cantilever has a spring constant of $k_0 = 7 \cdot 10^{-5}$ N/m, an effective mass of $m_{eff} = 2.0 \cdot 10^{-13}$ kg [13], a resonance frequency of 3.0 kHz and a quality factor (Q-factor) of $Q = 30000$ when far away from the sample's surface. The resonance frequency and Q-factor can be extracted from a Lorentzian fit to the cantilever's frequency response while

[1] CF-650, Leiden Cryogenics, The Netherlands

[2] MQP-S-11-9-20001-070 isotropic powder by Magnequench, Singapore

driving the cantilever around its resonance frequency. The NdFeB particle is magnetized in the x-direction at room temperature at a magnetic field of 5 T, and can be approximated as a spherical dipole. Subsequently, the particle obtained its saturation magnetization of 1.15 T and serves as the static magnetic field (B_0) source. The B_1-source nessecary to manipulate the spins in the sample under study is provided by sending a radio frequency (RF) current with a function generator [3] through a superconducting niobium titanium nitride (NbTiN) [3] micro-wire (RF-wire).

The cantilever is glued to a cantilever holder which can be actuated by a piezoelectric element. The piezoelectric element is connected to the output of a lock-in amplifier [4] and is used to drive the cantilever. Subsequently, the motion of the magnetic particle creates a magnetic flux change in a nearby superconducting pick-up coil. The change in magnetic flux induces a supercurrent in the pick-up coil which in turn is coupled via inductively matched transformers to a SQUID. The SQUID output is proportional to the cantilever's motion and is connected to the input of the lock-in amplifier. The SQUID serves as an extremely sensitive and low dissipative detector for flux changes, allowing MRFM experiments at millikelvin temperatures [14]. The SQUID noise (detector noise) is measured to be 5 $\mu\Phi_0$, where $\Phi_0 = \frac{h}{2e} \approx 2.068 \cdot 10^{-15}$ Wb is the magnetic flux quantum.

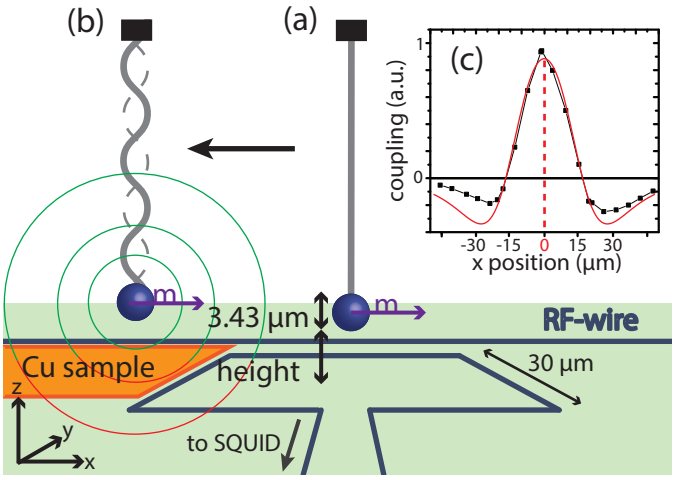

Figure 2.1: **Overview of the experimental setup.**
The MRFM set-up consists of a cantilever with a B_0-field source (magnetic particle) attached at its tip and a detection circuit (pick-up coil and SQUID). The sample under study is copper. An RF-wire provides the B_1-field nessecary for spin manipulation of the copper nuclei.

[3] Stanford Research Systems
[4] Zurich Instruments HF2LI

2.2 Calibration of the cantilever displacement

The amount of change in magnetic flux through the pick-up coil is proportional to the displacement x of the cantilever's magnetic particle. Hence, the cantilever displacement is related with the output of the SQUID according to $\langle x \rangle = \alpha \langle U \rangle$, where α is the coefficient of proportionality. Using the equipartition theorem, the cantilever's energy in thermal equilibrium is given by $\frac{1}{2} k_B T = \frac{1}{2} k \langle x \rangle^2$, from which follows:

$$\alpha = \sqrt{\frac{k_b}{k} \frac{\langle U \rangle^2}{T}} \tag{2.1}$$

where U is the output voltage of the SQUID and k_B is the Boltzmann constant. The output signal of the SQUID can be calibrated experimentally to a distance by measuring the squared area of the cantilever's thermal spectrum as function of cantilever temperature. Accordingly, $\langle U \rangle^2 T$ can be easily extracted as a fitting parameter from a linear fit. Figure 2.2 shows the average squared area of the cantilever's thermal spectrum for several temperatures, ranging from 50 mK up to 500 mK. Here, we recorded at least 25 thermal spectra at every temperature point. From a linear fit to the squared average area we find $\alpha = 11$ nm/mV$_{rms}$.

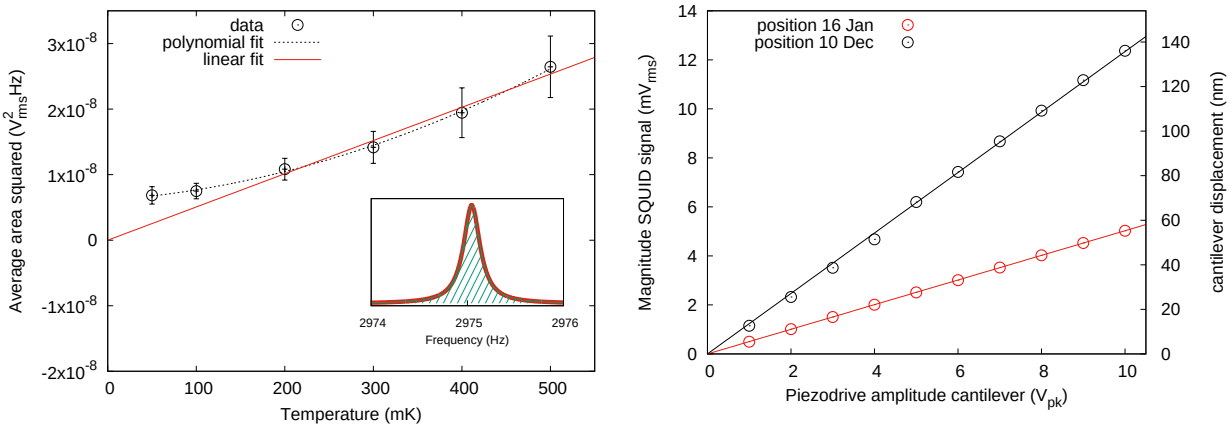

Figure 2.2: **Calibration of the cantilever displacement.**
Measurements where performed with the cantilever aligned far above the pick-up coil with maximal coupling, where Q = 30000. (a) Average squared area below a cantilever's thermal spectrum as function of cantilever temperature. At every temperature point, at least 25 thermal spectra were recorded. The slope of the linear fit to the data can be used to calibrate the SQUID output to a cantilever displacement, yielding 11nm/mV$_{rms}$. (b) Cantilever drive (piezoelectric) versus SQUID output for 2 different heights above the copper sample. The graphs correspond to the 2 cantilever locations where NMR experiments were performed. The calibration is used to translate the SQUID output to a displacement in nm.

2.3 Measuring an NMR signal

The NMR experiments are based on frequency shift measurements. Frequency shifts were measured with a lock-in amplifier and a digital phase-locked loop (PLL) control to keep the phase of the resonance frequency fixed. A single frequency shift measurement consists of the following sequence: The resonance frequency of the driven cantilever is measured with a PLL control for 3 seconds, after which the PLL is turned of and an RF current is turned on for an interval of t_p seconds (typical, $t_p = 1$ s). Finally, the PLL is turned on 1 second after the RF pulse is turned off. Accordingly, we wait for a period of at least 3 times the T_1 time before we start a new frequency measurement. Figure 2.2a shows a typical frequency shift measurement, where we have fit the data with 1.5, from which we can obtain the initial frequency shift as a fitting parameter. Furthermore, we fix the T_1 time according to the Korringa relation for copper, $T_1T = 1.1$ sK (ref.). The figure demonstrates that at least 30 averages are needed for a reliable fit. All NMR measurements were performed at a sample temperature around 70 mK and at several cantilever heights ranging between 3 and 4 μm, where the cantilever was aligned above the copper sample and sufficiently close to the RF-wire and pick-up coil. For these cantilever heights, the corresponding resonance frequency of the copper spins ranges between 200 - 900 kHz. Figure 2.2b shows that within this bandwidth the magnitude of the transfer function of the RF-wire decays linear for increasing frequencies. For RF frequency sweep measurements we corrected for this feature such that we obtained a constant B_1-field strength. Using an infinite circular wire as a model for the RF-wire, we approximate that an RF current of 0.6 mA used within a typical NMR experiment corresponds to a field strength at $r = 7$ μm of $B_1 = \frac{\mu_0 I}{4\pi r} \approx 8.7$ μT. As pointed out by Wagenaar et al, the settings of the RF-wire as reported here are within the domain where no additional heat dissipation occurs.

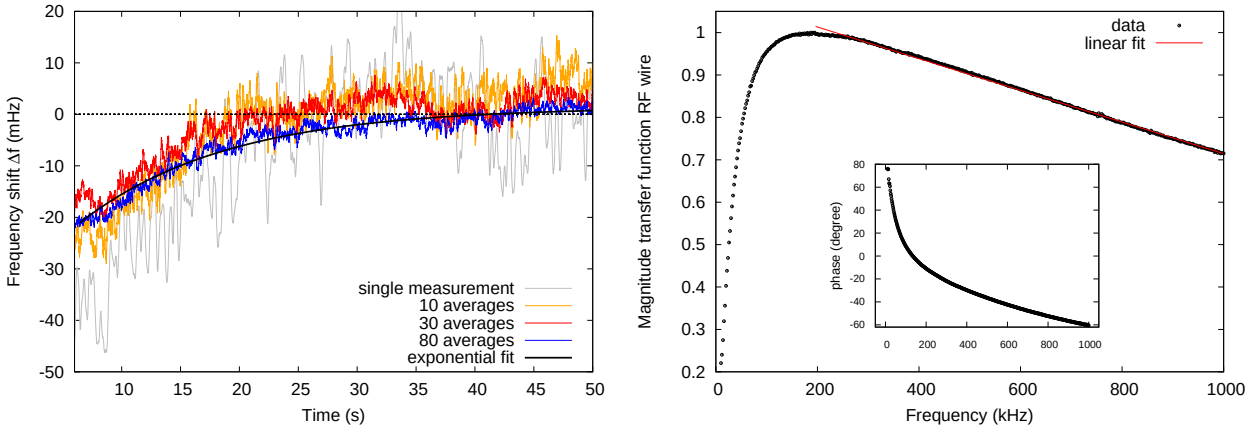

Figure 2.3: **Example of a frequency shift measurement.**
(left) A typical NMR measurement at 71 mK. The data is fitted to equation 2.1, using $T_1 = 14.9$ s and the initial frequency shift as a free parameter. (right) The transfer function of the RF-wire, which is used to calculate the B_1 field that is generated by the RF current.

2.4 Noise within an NMR measurement

The noise that is present in a typical NMR measurement is well described by Wagenaar [15]. To briefly summarise his description, the total frequency noise power spectral density (PSD) that is present during a frequency shift measurement is given by:

$$S_{\Delta f}(f_m) = \frac{4k_B T Q}{2\pi A^2 k_0 f_0}\left(\frac{f_m^2}{1+(\frac{2Qf_m}{f_0})^2}\right) + \frac{S_{det}}{A^2}\left(f_m^2 + \frac{f_0^2}{4Q^2}\right) \tag{2.2}$$

where T is the cantilever temperature, A is the cantilever driving amplitude and S_{det} is the PSD of the detector noise. The first term on the right-hand side represents the thermal noise. The second term originates from the detector noise and is determined by measuring the noise floor of the thermal spectrum of the SQUID. Using the calibration as reported in section 2.2, the detector noise is measured to be 82 pm/$\sqrt{\text{Hz}}$. We took into account that the modulation frequencies are small compared to the cantilever's resonance frequency ($f_m \ll f_0$).

Figure 2.4 shows the PSD of the frequency noise as a function of modulation frequency for piezoelectric-driving. Measurements were performed at a sample temperature of 70 mK and at a cantilever height close (x μm) and relatively far (y μm) above the copper sample. From the figure it is clear that more frequency noise is present at a cantilever height close to the copper. The difference in noise level is due to a drop in the cantilever's quality factor when the cantilever's magnetic particle is approaching the copper surface. We attribute this observation to the presence of Eddy currents in the copper sample, which introduce an additional damping source. The Eddy currents might also explain the observed $1/f$ noise, although the origin of the $1/f$ noise requires a more thorough study.

Using a PLL bandwidth of 10 Hz, the PSD spectra were recorded for several cantilever driving amplitudes. As expected from equation 2.1, the noise level is observed to be lower for higher driving amplitudes. Since the $1/f$ noise is present up to 5 Hz, the spectra could not be fit to equation 2.3. However, equation 2.3 fits well to PSD spectra where we used a 100 Hz PLL bandwidth. Here all fitting parameter were fixed to their known values. Although the sample temperature during the measurement was 70 mK, the temperature parameter was fixed at 139 mK since the thermodynamic mode temperature of the cantilever saturates at this temperature (Den Haan, 2016). Since NMR frequency shift measurements are of the order mHz, it is clear from the PSD spectra that one needs to take many averages to obtain a sufficient signal to noise ratio.

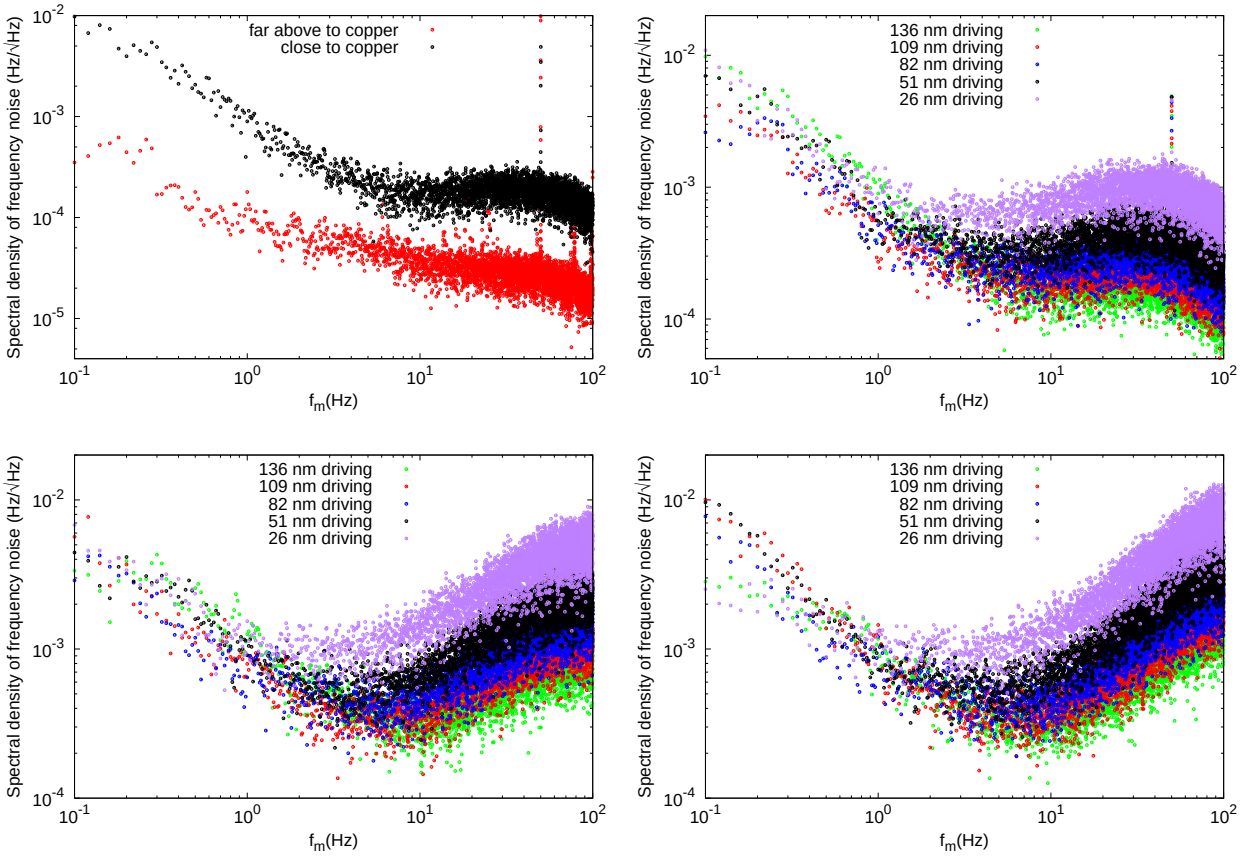

Figure 2.4: **Noise frequency spectra of a frequency shift measurement.** All spectra correspond to an average of 5 individual noise spectra. (a) A PSD spectrum recorded close (black) and far above (red) the copper sample. Here, the PLL bandwidth is set to 10 Hz and the cantilever height is respectively x and y μm. We attribute the increase in noise intensity at a smaller cantilever height to a stronger interaction between the cantilever's magnetic particle and the Eddy currents in the copper sample. Up to 5 Hz, a clear $1/f$ noise is visible, which limits the frequency shift measurements since the corresponding signals are of the order 10 mHz. The sharp peek at 50 Hz is due to the 50 Hz noise. No additional noise at the pulse tube frequency (1.4 Hz) is visible. (b) PSD spectra at x μm for several driving amplitudes and a PLL bandwidth of 10 Hz. As expected from equation 2.1, the noise decreases with increasing driving amplitude. (c) Idem, only now we have set the PLL bandwidth to 50 Hz and (d) 100 Hz.

Chapter 3

Results

We report on local NMR measurements of copper at millikelvin temperatures. In particular, we observed a strong amplification of the NMR signal in the case that the Larmor frequency of the copper nuclear spins approach a higher resonance frequency of the cantilever. A better understanding of this phenomenon requires a characterization of the cantilever's higher resonance modes. Therefore, the cantilever's transfer function has been studied for several higher modes and for different driving amplitudes. Taken together, we were able to reproduce the findings of Den Haan and Wagenaar [16] and we have shown extended evidence for their proposed ABCD model.

3.1 Characterization of the resonance modes

In order to understand the effect of a higher resonance mode on an MRFM signal, it is critical to have knowledge about the cantilever's frequency response within the domains where resonance occurs. In the upcoming subsection we will show that we have identified six higher resonance frequencies. Two higher modes, which correspond to the regime where we performed local NMR measurements on copper, are studied with respect to the cantilever's driving amplitude and coupling to their higher harmonics. The results of the latter two studies are reported respectively in subsection 3.1.2 and 3.1.3.

3.1.1 Identification of the resonance frequencies

The undamped resonance frequencies of the cantilever are modelled by a finite element analysis with COMSOL Multiphysics 5.0, using an eigenfrequency study. Figure 3.1 shows the modes' shapes and resonance frequency as predicted by this computer model. Simulation parameters are specified in this figure.

By sending an alternating current through the superconducting RF wire to drive the cantilever, the frequency response of the cantilever is recorded with a lock-in amplifier while sweeping the RF frequency around the expected resonance frequencies.

Accordingly, Bode plots of the recorded spectra were used to identify at which driving frequencies resonance occurs. Table 3.1 demonstrates that the resonance frequencies of all transient modes up to 1 MHz were found within 10 percent deviation of the modelled undamped resonance frequencies. Here, all higher modes were identified at relatively higher frequencies.

Although the finite element analysis did not include damping, we should not ignore its contribution within measurements. An important indication for the amount of damping can be determined by measuring the Q-factor of the fundamental mode. At the cantilever height of 3 μm where all higher resonance frequencies were recorded, a Q-factor of 500 was subtracted from a Lorentzian fit to the measured transfer function of the cantilever's fundamental mode.

Mode	**Simulation** [kHz]	**Experiment** [kHz]	**Deviation** [%]
1	3.043	3.034	0.30
2	32.8	33.5	2.17
3	101.9	103	1.06
4	112.2	-	-
5	207.9	208	0.06
6	274.0	-	-
7	347.2	361	3.99
8	511.0	540	5.68
9	698.49	759	8.66
10	918.95	-	-

Table 3.1: **Resonance frequencies as predicted and as found in experiment.** The cantilever is driven by the RF wire and the cantilever's frequency response is recorded accordingly. Non-transient modes (modes 4, 6 and 10) were not observed. We attribute the deviation between the predicted and observed resonance frequency mainly to the absence of modelled damping in the COMSOL model. Measurements were performed at a cantilever-magnet height of x μm.

In comparison with the Q-factor of 30000 which has been measured far above the copper and at maximum coupling to the pick-up coil [11], we can conclude that at this height, additional damping besides material damping enters the system. This might explain the observed deviation between measured and modelled resonance, which also increases with frequency. We attribute this observation to the copper sample in the vicinity of the cantilever's magnetic particle: the additional damping is induced by Eddy currents which are known to be more present with increasing frequencies (ref).

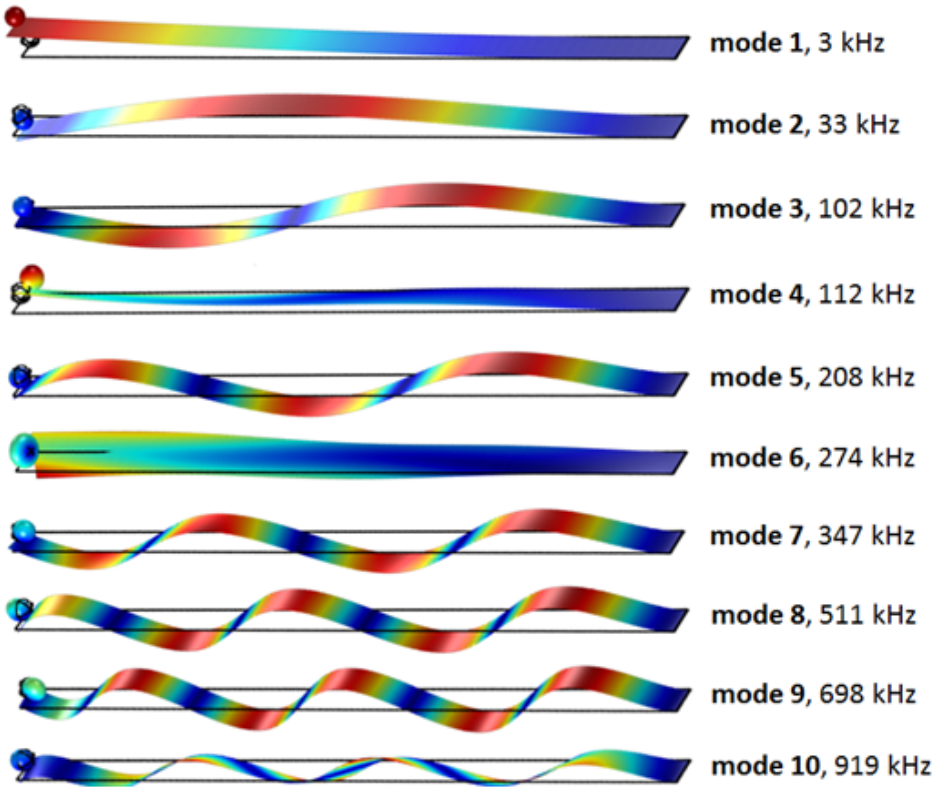

Figure 3.1: **All mode shapes of the cantilever within the** kHz**-domain.**
The mode shapes are modeled by a finite element analysis (COMSOL Multiphysics) using an eigenfrequency study. The colour gradient gives an indication of cantilever displacement, where the red coloured regimes are the locations where we expect the most significant modal displacement and the blue coloured regimes represent minimal motion. Three modes (mode 4, 6 and 10) are non-transient modes and were therefore not detected. It is important to note that the dynamics of the magnetic particle at transient higher modes are mainly rotational, which is due to the relatively larger mass of this particle compared to the bare silicon cantilever. Parameters for the simulation are beam length: 140 µm, beam width: 4.51 µm, beam height: 0.1 µm, magnetic particle's radius (modelled as a sphere): 1.725 µm, number of mesh elements: 11474.

Furthermore, three higher modes (mode 4, 6 and 10) were not detected in this experiment. This can be explained by their corresponding mode shape which mainly evolves perpendicular to the transient direction instead of parallel.

In the following two sub-sections we will pay extra attention to mode 8 and 9 (measured around 540 kHz and 759 kHz respectively). The dynamics of the magnetic particle at these two higher modes will play an important role within the NMR experiments that are described in section 3.2. From the mode shapes depicted in figure 3.1 we deduce the tip motion at these modes is mainly rotational, due to the relatively larger mass of the magnetic particle compared to the mass of the bare silicon beam.

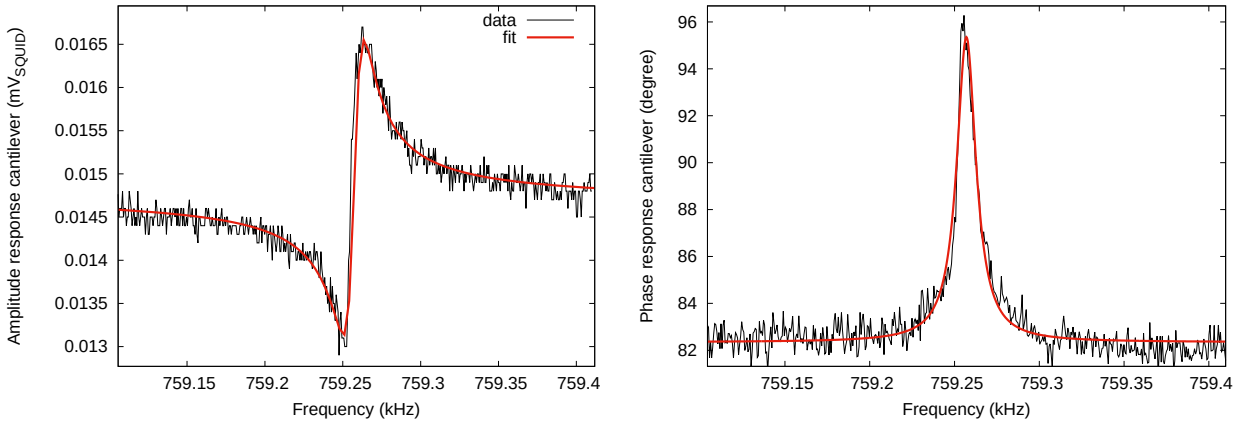

Figure 3.2: **Example of a bode plot - amplitude and phase - of a higher mode.** The measured response is fitted with the calibration transfer function - equations 4.23 and 4.24 - as reported by reference [10]. (left) The transfer function (amplitude) measured at mode 9 where a low RF current of 500 V was used to drive the cantilever at this mode. A similar behaviour was observed for other higher modes. (right) Idem, phase mode 9. Fit parameters: $\Omega^{'} = 759256$ Hz, $\Omega_T = 759258$ Hz, $\beta^2 = 5.27 \cdot 10^{-5}$.

3.1.2 Modal analysis for increasing driving amplitudes

The cantilever's response at several resonance modes were studied with respect to the cantilever's RF-drive amplitude. For RF currents larger than 1 mV the higher modes show a typical Duffing-oscillator response, also known as the *foldover effect* [17]. Figure 3.3 shows that this behaviour is clearly visible from the shift in resonance frequency and the hysteresis observed in a forwards and backwards sweep.

The characteristic distortion of the resonance curve originates from non-linear mechanical properties (i.e. non-linear material stiffness) which are described by a non-linear term in the Duffing equation. This contribution become more dominant for large driving amplitudes. We note that the foldover effect can be used for fast identification of the cantilever's

resonance frequency, by searching for a sharp step in the cantilever's phase while backwards sweeping and using a large driving amplitude.

The shape of the transfer function of the fundamental and higher modes differs from the typical Lorentzian response/π-phase shift observed for the fundamental mode when exciting the cantilever with a piezoelectric element. A similar behaviour was observed for the excitation of the fundamental mode with the in-circuit integrated calibration coil (Wijts, 2013). Although the measured transfer functions of mode 9 fit well to this model (see figure 3.2), a more thorough study is required for complete understanding of the cantilever's driving mechanism while using the RF-wire.

For the MRFM set-up we described in section 2, the minimal amplitude of the RF current that is needed for the generation of B1 field strengths necessary for a typical NMR experiment, is of the order 100 mV. We have shown that radio frequencies of this order of magnitude are accompanied with a highly non-linear behaviour of the cantilever. As a consequence, for NMR experiments where the frequency of the RF-current correspond with the region of bistability as described in table 3.2, we could expect a response due to the rotation of the magnetic particle which dynamics is dependent on the history of the cantilever's driving amplitude.

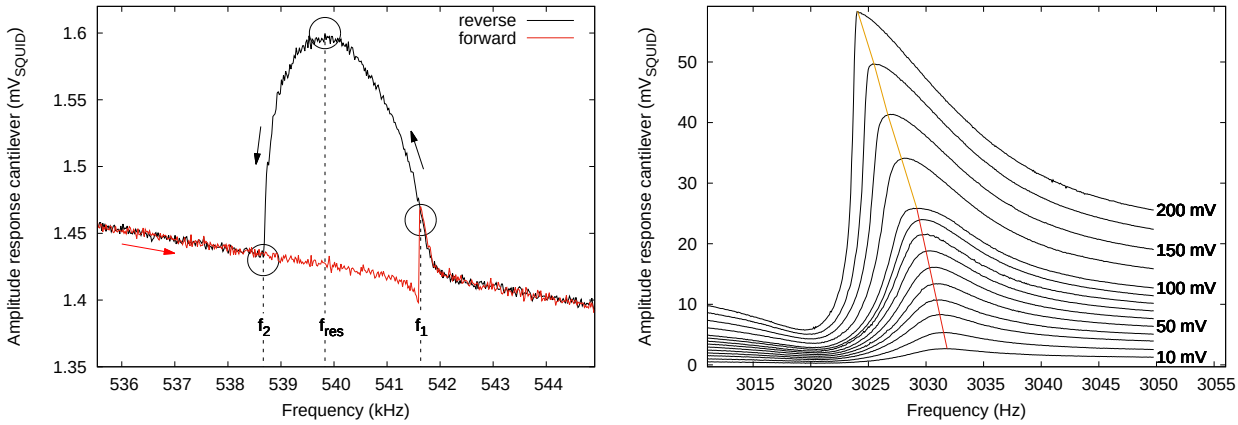

Figure 3.3: **Modal response for large RF driving amplitudes.**
(left) Frequency response at mode 8. Driving amplitudes larger than 1 mV show a distortion of the resonance spectra (foldover effect) which is clearly visible from the characteristic jump phenomenon and observed hysteresis in a forward and backward sweep. Here, a driving amplitude of only 20 mV was used. (right) As a reference, the frequency response for several driving amplitudes of the fundamental mode is shown (10 mV up to 200 mV). At this mode, the foldover effect is less dominant compared to the higher modes, and appears at larger driving frequencies. The shift in resonance frequency (indicated by the red line) shows a linear behaviour, although driving frequencies larger than 100 mV show a steeper trend (yellow line).

A_{RF} (mV)	f_{res} (kHz)	f_1 (kHz)	f_2 (kHz)
50	535.05	541.51	531.93
70	531.49	541.45	531.45
100	531.51	541.39	531.45
130	531.51	541.39	531.45

Table 3.2: **Region of bistability at mode 8 for NMR driving amplitudes.** When driving the system with a driving amplitude larger than a certain critical value (here 1 mV), the region is defined for $f_2 \leq f_{drive} \leq f_1$ and corresponds to the frequency domain where the system shows the behaviour of an anharmonic oscillator. For very large driving amplitudes, the region size saturates to a maximum value. The same behaviour is observed for the shift in resonance frequency. Similar observations were found for mode 9 and other cantilever heights. The drive amplitudes shown here correspond with the amplitude of the RF pulses used in the NMR experiments that are described in the next section.

3.1.3 Anharmonicity study

Oscillating systems where the stiffness is not independent of the system's driving amplitude - and thus do not obey Hooke's law - are known as *anharmonic-oscillators*. In the previous subsection we saw that Hooke's law breaks down for RF driving amplitudes larger than 1 mV. Accordingly, the system responds in a non-linear fashion which result in an asymmetric modification of the cantilever's frequency response at resonance and the resonance frequencies are shifted with respect to their natural resonance frequencies. This frequency shift dependency as function of driving amplitude is a direct measure of the non-linear properties of the system, and is shown for mode 8 in figure 3.4a. This result implies that the cantilever is softening with driving amplitude, since the resonance frequency is decreasing for larger driving. The frequency shift is measured for mode 8 and 9 and for the cantilever being in the vicinity/far above the copper sample to see whether the non-linear character could be attributed to Eddy currents. Comparing the behaviour at both scenarios, the measurement shows a small deviation in frequency dependence. From this we can conclude that the interaction between the cantilever and the sample is not responsible for the observed non-linear character, which leaves the geometry and material properties of the cantilever as the main sources for the non-linear behaviour.

An important remark here is that the curve that is measured is not understood completely, since we expected a quadratic decrease in resonance frequency while increasing the driving amplitude (ref). Although far above the copper we indeed observe this dependence for small driving frequencies, for larger driving frequencies we measure a linear decreasing dependence that saturates at a final value. A more thorough discussion of this observation is reported in chapter 4.

Furthermore, within the non-linear regime, the energy that is stored into a specific resonance mode could be coupled to vibrations at other modes and frequencies, such as frequencies that corresponds to a higher harmonic of this resonance mode. For resonance modes

1, 7 and 8, the coupling between the first, second and third harmonic has been studied as function of RF-drive amplitude. Using the lock-in amplifier to drive the system at the first harmonic of one of these modes, the response at the first two higher harmonics was measured simultaneously for increasing driving amplitudes. The results, shown in figure 3.2, demonstrate that there exists a small coupling between the first 2 harmonics of the fundamental mode, but negligible coupling between the higher harmonics of modes 8 and 9.

Coupling of a resonance mode to higher modes has not been studied yet for driving the system using an RF wire. However, the coupling between mode 1 and 8 has been studied for piezodriving up to piezodriving voltages of 350 mV. Within this study, a digital Phase-Locked-Loop (PLL) control was used to excite the cantilever at mode 8 as function of piezo-drive amplitude. Accordingly, a thermal spectrum of the fundamental mode and the amplitude of the PLL-signal were recorded. Using the calibration as reported in section 2, we find a maximal cantilever displacement of 0.66 nm at a piezodriving amplitude of 250 mV, after which the displacement saturates. The saturation behaviour is in accordance with the saturated frequency shift at 250 mV found by Den Haan (Haan, 2016). These findings show limited coupling between a higher resonance mode (mode 8) and the fundamental mode. Whether this conclusion is still valid within the experimental environment of the NMR experiments that we will describe in the next session, we remark that a similar study needs to be performed when driving the system using an RF-wire.

3.2 Local NMR measurements on copper

In this section we report on local NMR measurements on copper nuclear spins at millikelvin temperatures. The NMR signal originates from a change in the spin-cantilever interaction due to spin manipulation initiated by an RF-pulse. Accordingly, a change in interaction results in a change in the cantilever spring constant. As a direct consequence, the fundamental resonance frequency of the cantilever is shifted. Frequency shifts were measured with a lock-in amplifier and a digital PLL control to keep the phase of the resonance frequency fixed.

3.2.1 Amplification of B_1 by cantilever displacement (ABCD)

Figure 3.5a shows an example of a measured frequency shift after sending an RF pulse (542 kHz, 200 mV). Here, we used a pulse-width of $t_{pulse} = 1$ s, which is sufficiently long to saturate all Boltzmann populations within the resonance slice: the volume where the RF-frequency matches the Larmor frequency of the nuclear spins: $hf_{RF} = \gamma B(\mathbf{r})$. As a result, the interaction between the spins within this slice and the cantilever is completely lost and a frequency shift is observed. Subsequently, the system relaxes back to equilibrium

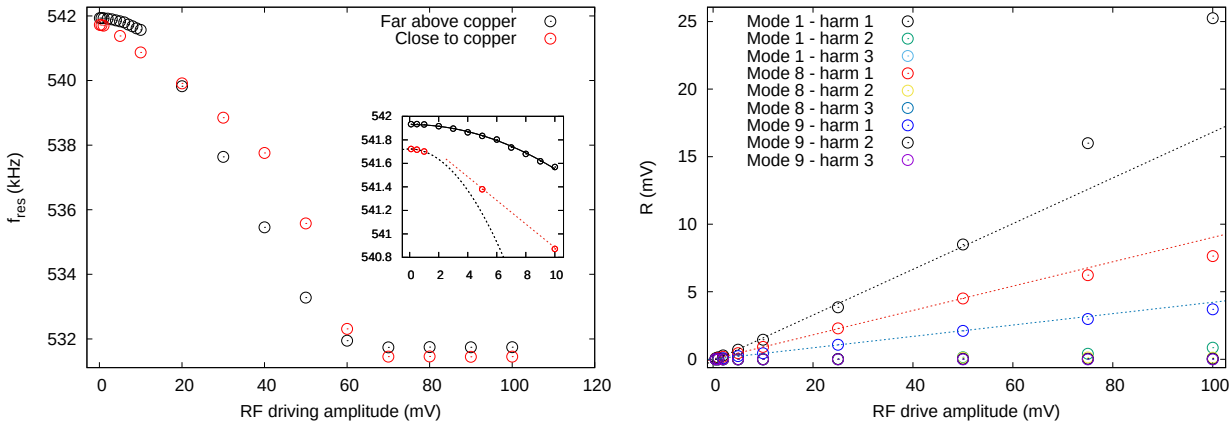

Figure 3.4: **Non-linear behaviour and coupling to higher harmonics.** (left) A frequency shift as function of driving amplitude at mode 8. The decrease in resonance frequency shows that the cantilever is softening for large driving amplitudes. The shift behaves quite similarly for the cantilever being close and far away from the copper sample, indicating that Eddy currents are not a major source of the non-linear character. (right) Coupling between a resonance mode and its higher harmonics. For mode 1, 8 and 9, the cantilever is excited at its first harmonic and the system's response (R-value of the SQUID signal) is measured at the 1^{st}, 2^{nd} and 3^{rd} harmonic of this mode respectively. The results show limited coupling between a resonance mode and its higher harmonics.

(the unperturbed Boltzmann population), where the relaxation rate is characterised by the spin-lattice (T_1) decay process.

All NMR measurements were performed at a sample temperature around 70 mK. At these temperatures, a T_1-time 16 seconds was extracted from a single exponential fit, and corresponds well with the expected T_1 time according to the Korringa relation for copper $T_1T = 1.1$ sK (Wagenaar et al.). We used the initial frequency shift as a fitting parameter. Further experimental settings are described in the figure caption.

The cantilever height above the copper sample was tuned such that a coupling between the nuclear spins and the cantilever's magnet is accomplished. Accordingly, a maximal NMR signal - and hence a maximal frequency shift - which corresponds to a maximal resonance slice within the copper sample, was predicted by using a simulation as reported by de Voogd (de Voogd et al.). At a fixed cantilever height, the maximum shift is determined by the RF frequency and the field gradient. As an increasing function of RF frequency, the resonance slice will enter the copper sample up to a maximum volume, and will leave the sample subsequently.

Figure 3.5b shows the RF frequency dependency found in experiment for a cantilever height of 3 μm. The experiment is in agreement with the simulation and for this height, a maximal frequency shift is observed around 542 kHz. However, as was first noted by Den Haan and

Wagenaar [16], a finer sweep around this maximum reveals an extra factor 2 frequency shift than expected by simulation. The frequency region where this amplification of the signal takes place corresponds well to the resonance region of mode 8 (see table 3.2). From this we can conclude that the observed amplification is due to the higher mode cantilever vibration.

We attribute the source of the enhanced frequency shift to the extra B_1-field that is generated from the rotational motion of the cantilever magnet. Concerning terminology, we will refer to this phenomenom as 'Amplification of B_1 by cantilever displacement', abbreviatiated as ABCD.

In the next subsection we will show the results from NMR experiments in which we studied the ABCD effect at mode 8 and mode 9.

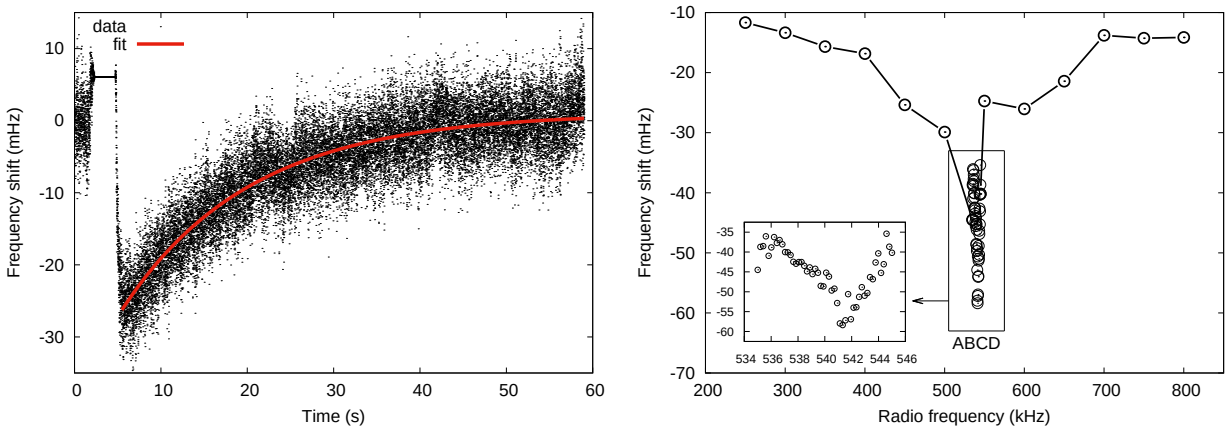

Figure 3.5: **Amplification of B_1 by cantilever displacement (ABCD).**
The Boltzmann populations of the nuclear copper spins are completely saturated within a specific resonance slice after a 1 second RF pulse with corresponding frequency is exposed to the copper sample. (left) A typical frequency shift measurement. The data represents an average of 80 single measurements, where we waited 60 seconds in between two pulses. Further experimental settings are: T_{sample}: 71.8 mK, PLL drive amplitude: 8 V, RF driving amplitude: 200 mV. (right) Frequency shift as function of RF frequency. The lines joining the points are guides to the eye. As an increasing function of RF frequency, the resonance slice will enter the copper sample up to a maximum volume, and will then leave the sample again. The data shows an additional frequency shift around the frequency domain where a higher mode (mode 8) of the cantilever is excited. We attribute the extra signal to the generation of an additional B_1-field (ABCD), due to the higher mode vibration of the magnet. Further experimental settings are: 80 averages sweep 200-800 kHz, 45 averages sweep 534 - 546 kHz, T_{sample}: 71.5 mK, PLL drive amplitude: 8V, RF driving amplitude: 200 mV.

3.2.2 Rabi oscillations

Figure 3.6 shows NMR measurements for millisecond RF pulses. At this time scale, the observed oscillating behaviour, well-known as *Rabi oscillations*, demonstrates that the Boltzmann populations are not fully saturated. From the Rabi flopping frequency we can extract the B_1 field-strength, using the relation $B_1 = \gamma^{-1} h f_{Rabi}$.

The figure shows Rabi oscillations measured at two differents heights, corresponding to the RF frequency where we expect ABCD at mode 8 and mode 9. Accordingly, for a gyromagnetic ratio of 11.54 MHz/T, we find a B_1-field strength of 42 μT and 35 μT respectively. The deviation of approximately 17% in field-strength could be attributed to a smaller magnet rotation at mode 9 compared to the rotation at mode 8.

Furthermore, in accordance with the findings of Den Haan and Wagenaar [16], the Rabi oscillations seem to saturate for both modes for a pulse length longer than 8 ms.

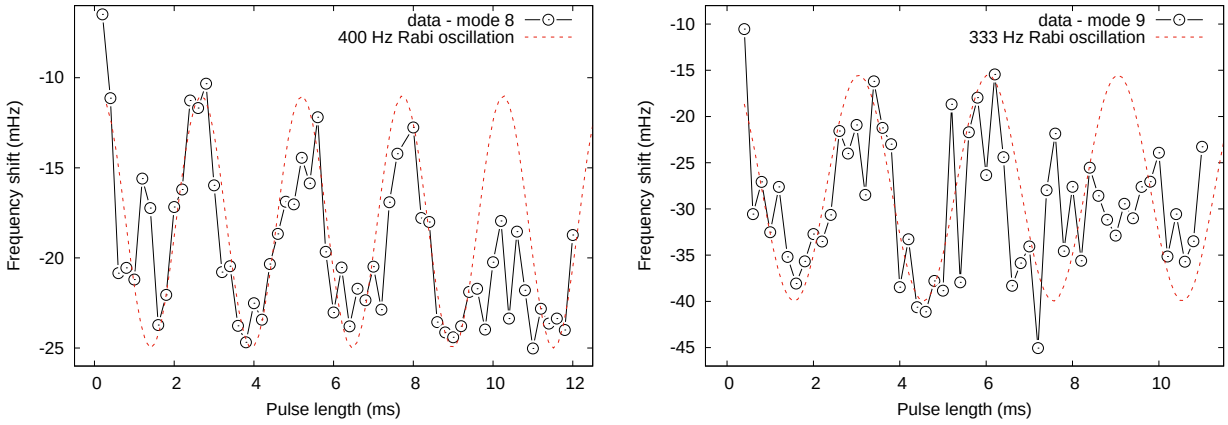

Figure 3.6: **B1-field strenght at ABCD as measured for mode 8 and 9.**
The figures show measured frequency shifts at a time scale where the Boltzmann populations are not saturated yet, allowing the monitoring of Rabi oscillations between the different spin states. Each point represents an average of 30 single frequency shift measurements. The lines joining the points are guides to the eye. Measurements were performed at 2 different heights, corresponding to an RF amplitude where the maximal frequency shift matches with the resonance frequency of mode 8 and mode 9 respectively. From the period of the Rabi oscillation, a value for the B_1-field strength can be extracted. (left) Rabi oscillations at a cantilever height where the maximal frequency shift corresponds to mode 8. Experimental settings: sample temperature: 72 mK, RF-drive amplitude (541220 Hz): 100 mV, PLL drive amplitude: 8V. (right) Idem, for mode 9, sample temperature: 66 mK, RF-drive amplitude (759225 Hz): 100 mV, PLL drive amplitude: 10 V.

Figure 3.7 shows how Rabi oscillations at mode 8 are modified when using other RF-driving amplitudes and PLL voltages. As expected, the results show a halving of the frequency shift when driving the cantilever with half the amplitude, since the 3 kHz cantilever and hence resonance slice motion is doubled in amplitude. However, for an RF amplitude of 50 mV and 70 mV we observe *faster* Rabi oscillations than at RF driving amplitudes of 100 and 130 mV. We attribute these observations to the non-linear response of the higher resonance mode, although a more thorough analysis is needed to confirm this hypothesis. Further peculiar observations which are not understood completely are discussed in further detail in the next chapter.

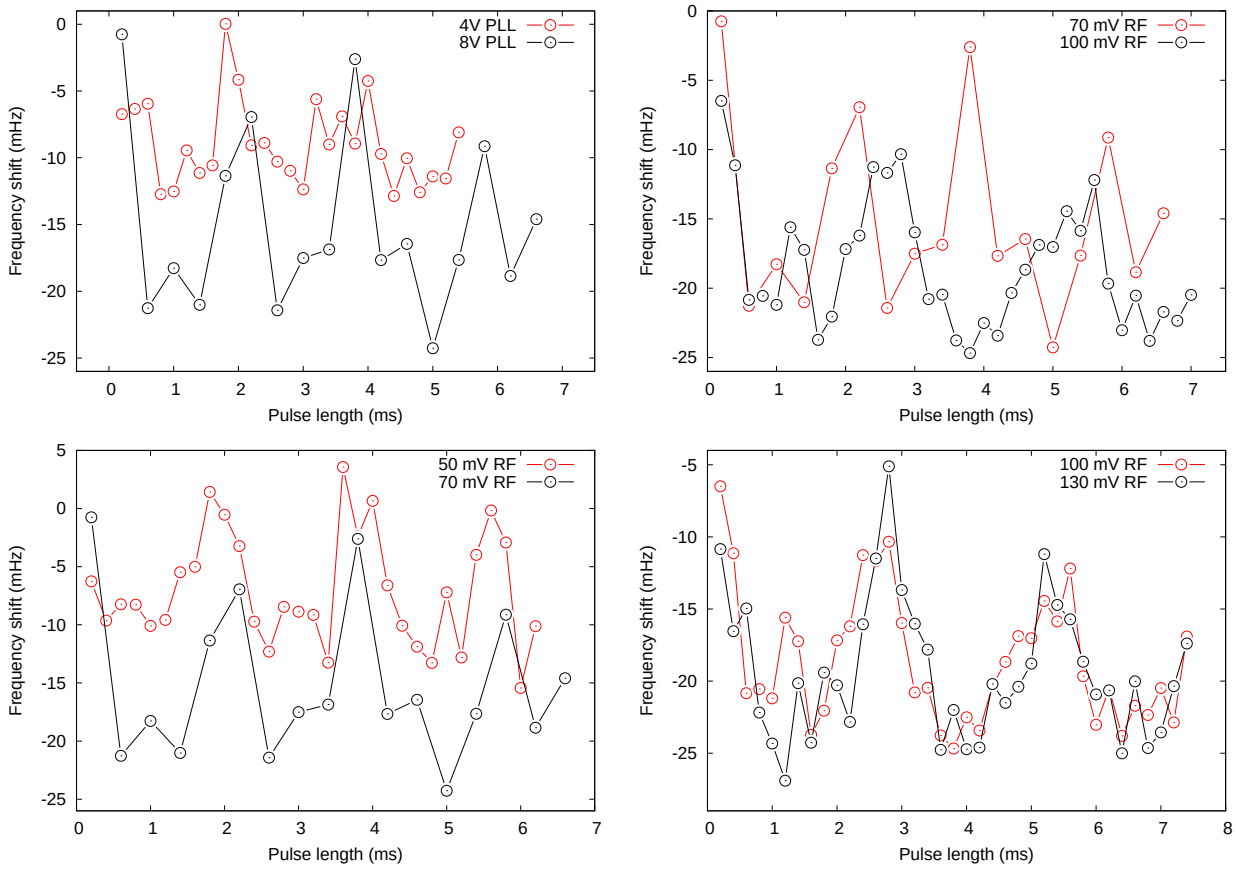

Figure 3.7: **Rabi oscillations examined for cantilever and RF drive amplitude.** The measurements were performed at a cantilever height where the maximal frequency shift corresponds with mode 8. Each point represents an average of 30 single frequency shift measurements. The lines joining the points are guides to the eye. (left top) For a twice as low PLL piëzo cantilever drive amplitude, we observe an unchanged Rabi frequency, which was expected since the same RF pulse settings were used in both measurements. Furthermore, a larger PLL driving amplitude will broaden the resonance slice, which is reflected in a larger frequency shift. The figure shows indeed that the frequency shift scales with the cantilever driving amplitude. Experimental settings: sample temperature: 69 mK, RF-drive amplitude (541220 Hz): 70 mV. (right top and bottom) The figures show that the Rabi frequency does not scale with the RF driving amplitude. We attribute this unexpected behaviour to the non-linearity of mode 8. A more detailed discussion about this observation is reported in Chapter 4. Experimental settings: sample temperature: 69 mK, RF-drive frequency: 541220 Hz, PLL drive amplitude: 8 V.

Chapter 4

Discussion

In the previous chapter we have shown the results of local NMR measurements on a copper sample at millikelvin temperatures, where we have recorded the change in the fundamental resonance frequency of the cantilever due to a change in magnetic coupling between the cantilever's magnetic particle and the magnetic moment of the copper nuclei in the resonance slice. The data show an additional frequency shift by more than a factor 2 in the special case that the Larmor frequency of the nuclear spins within the resonance slice matches a resonance frequency of the cantilever's higher transient eigenmode. We contributed this amplification of the NMR signal to the additional B_1-field generated by the rotational vibration of the magnetic particle, which is induced by the actuation of the corresponding higher resonance mode of the cantilever. This data interpretation is build on the assumption that the measured frequency shifts correspond to an NMR signal of the copper nuclei. In this section, we will provide a set of arguments that support this claim and the subsequently data interpretation. Furthermore, we will discuss the interpretation of the Rabi oscillation measurements in further detail.

Spin heating versus NMR signal

Due to the temperature dependence of the spin polarization, the magnetic coupling between the cantilever and the copper nuclei is affected by temperature changes of the spin ensemble. Consequently, the cantilever's fundamental resonance frequency is shifted by temperature fluctuations of the copper sample and is measured to be 100 mHz/mK. This feature (spin heating) may disguise the NMR signal obtained within frequency shift measurements if the power dissipation of the RF-pulse is sufficiently large. Despite the use of a superconducting RF-wire, a very low but non-zero power dissipation is generated in type-II superconducting materials such as NbTiN [18], where vortices may play a dominant role within the creation of a dissipation channel. A recent study on the NbTiN microwire we used in our experiments shows at millikelvin temperatures as well as at 4.1 K a quadratically increasing power dissipation as function of current frequency[19].

Yet, for our current experimental set-up, we have observed no increase in sample temperature for RF-pulse lengths smaller than 5 seconds (when using an RF-driving amplitude of 200 mV) and for RF-driving amplitudes larger than 500 mV (when using a pulse length of 1 second), although the sample temperature might be higher since the sample temperature is measured and controlled *indirectly* via a thermalization bath [1] that is connected with the sample. Within the regime where we do measure sample heating, a clear frequency shift is observed with a relaxation behaviour that is similar to the NMR signal measured when no increase in sample temperature is measured. Although the typical currents we used within the NMR experiments (100 mV RF-driving amplitude and a 1 second pulse length) are far away from the regime where we observe sample heating, spin heating may still be induced during the RF-pulse. However, based on the following two arguments, we claim that the frequency shifts as measured and reported in section 3 correspond to the saturated and subsequently recovered magnetic moments of the copper nuclei: (1) The Korringa constant for copper as measured with the same set-up corresponds to the value as expected by literature [20]. (2) If the frequency shifts indeed *do* correspond with spin heating, figure 3.5 would not show the frequency dependency as was measured and expected by simulation. Instead, one would rather expect to observe a quadratically increasing frequency shift.

ABCD: proof of principle

We have contributed the enhancement of the maximal frequency shift to a higher resonance mode of the cantilever, since the frequency domain where we have measured a higher resonance mode matches one-to-one with the frequency domain where we observe an amplification of the expected NMR signal. Subsequently, we hypothesised that the rotational motion of the magnetic particle generates an additional B_1-field that increases the number of spins that are saturated. Den Haan and Wagnenaar have shown [2] that by solely driving the cantilever at the 8^{th} resonance mode by a piezoelectric element, a B_1-field of 30 μT was generated [16], where the corresponding rotational angle in the x-z direction of the magnetic particle was calculated to be $\theta = 0.07^\circ$ for a 100 mV driving amplitude. This angle is compatible with the angle we predict in our own model, which is somewhat oversimplified but useful for approximation (see Appendix A). The model is used to approximate the cantilever's tip angle at any transient resonance mode: Using equation A.13, we calculated for $Q_8 = 500$ a rotational angle of $\theta \approx 0.01^\circ$. Furthermore, in addition to figure 3.6, *no Rabi oscillations were observed* when using an RF-pulse matching the 8^{th} resonance mode at a cantilever height where the expected maximal frequency shift corresponds to the resonance frequency of the 9^{th} resonance mode, and vice versa, supporting our interpretation that the dynamics of the higher mode generates an additional B_1-field.

[1] The copper sample is connected to a wire bond copper pad, which is in turn connected via gold wire bonds to a sample holder. The Sample holder is thermelised via a welded silver wire to the 10 mK plate of the dilution refrigerator.

[2] paper in preparation

The Spin-Spin relaxation puzzle

In the last section of chapter 3, we showed the results from frequency shift measurements for RF-pulse lengths ranging between $0.2 - 12$ ms. The data correspond with damped Rabi-oscillations, from which we read the oscillation frequency to determine the amplitude of the B_1-field. However, this interpretation becomes problematic since the phenomenology of Rabi oscillations at this time-scale is difficult to reconcile with the spin-spin relaxation time (see 1.3) of copper: One would expect to observe exponentially decaying oscillations with a characterising decay time $\tau = T_2$, saturating at a certain frequency shift that corresponds to the saturated spin population ratio as limited by the saturation parameter $s = \gamma^2 B_1^2 T_1^2 T_2^2$ [21]. The problem becomes evident when we compare the measured decay time $\tau \approx 8$ ms with the known spin-spin relaxation time of copper, $T_2 = 0.15$ ms [22, 23]. The cantilever-spin interaction may alter the T_2-relaxation process, although one would expect that a certain interaction would contribute to *faster* relaxation rates. For instance, the thermal noise of the higher cantilever modes within the region of the Rabi frequency could serve as an additional relaxation channel [24]. However, as far as we are aware, no mechanisms are known or reported in which the T_2 lifetime of a spin system is significantly extended.

The problem described above will be further investigated within a separate research project, in which the complete spin-cantilever interaction will be modelled. The following ingredients may form a key to a better understanding of this spin-spin relaxation puzzle:

(1) The amplitude of the field-gradient could affect the Rabi-oscillation. To demonstrate this, figure 4.1 shows a Rabi oscillation that originates from a non-interacting spin-1/2 system within a field gradient. Transitions between the energy levels of nuclei that precess with a frequency close to the Larmor frequency can still be induced, although with a significantly lower probability than nuclei spins at perfect resonance ($\Omega = \Omega_R \Leftrightarrow \Delta = 0$). Furthermore, off-resonance spins contribute to faster Rabi-oscillations.

(2) The 3 kHz-motion of the cantilever during the RF-pulse may influence the spin dynamics. Based on the fundamental cantilever's ring down time $\tau = Q/f_{res} \approx 0.17$ s ($Q = 500$), we expect a combined motion of the cantilever's fundamental and higher mode during millisecond RF-pulses. Therefore, spins at the edge of the resonance slice are expected to experience a very different excitation/relaxation process.

(3) Non-linearities of the cantilever might complicate the mechanical motion of the cantilever, and thereby the cantilever-spin interaction. Theoretically, including the full non-linearities of the cantilever significantly increases the complexity of the problem, although the application of a simple Duffing model within the equation of motion might capture the cantilever's mechanical behaviour during the RF-pulse.

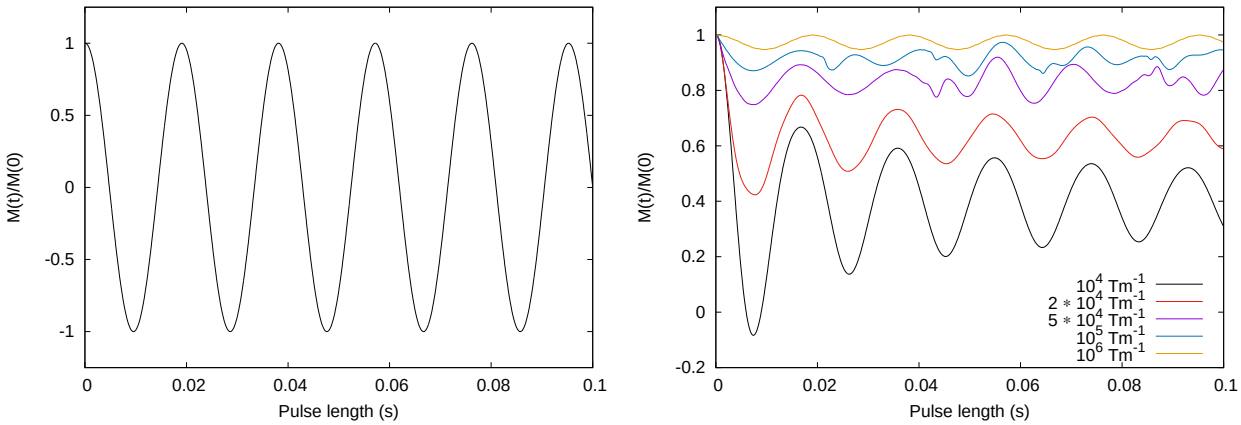

Figure 4.1: **Simulation of Rabi oscillations in a magnetic field gradient.** The simulation represents a simple model of copper nuclei in the resonance slice and is modelled as an $N \times M$ non-interacting spin-1/2 lattice ($N = 39, M = 3.5 \cdot 10^7$) with a lattice constant of ~ 3 Åm. Further simulation parameters are: $\gamma = \gamma_C u \sim 11 \cdot 10^6$ rad $\perp$ sec /T, $B_0 = 50$ mT (at the center of the lattice). The spins experience a magnetic field, which field strength increases linear with row-number N. Using equation 1.1, we determined the net magnetization as function of time, $M(t)/M(t = 0)$. (left) Setting $\frac{\partial B_1}{\partial z} = 0$, the net magnetization completely 'flips' periodically and the period corresponds to the total Rabi frequency $\Omega_R^2 = \Omega^2 + \Delta^2$, where $\Delta = 0$. (right) The Rabi oscillations are affected when we introduce a field gradient. The figure demonstrates that, as expected, for a relatively large field gradient ($\frac{\partial B_1}{\partial z} > 10^5$ T/m), only a small part of the complete spin population oscillates between the two allowed energy levels. This results in a small oscillation of the net magnetization. However, for applying an intermediate field gradient ($\frac{\partial B_1}{\partial z} \sim 10^4$ T/m), spins that precess at a frequency close to the Larmor frequency have a non-zero probability to absorb/emit with a larger frequency, since $\Omega_R^2 = \Omega^2 + \Delta^2$, where $\Delta > 0$. Consequently, the oscillation frequency of the net magnetization is increased, but also *damped*, a result we did not expect.

Chapter 5

Conclusion and Outlook

In this thesis we have demonstrated a new MRFM measurement protocol where we used a higher transient resonance mode of the MRFM force sensor to generate an amplification of the B_1-field. We have shown that the correct implementation of this feature within local NMR measurements on copper nuclei resulted in an amplification of the obtained NMR signal by more than a factor 2. Combined with the earlier findings of our colleagues Den Haan and Wagenaar [16], these results support our claim that a cantilever's higher mode can serve as an additional B_1-source: By solely driving the cantilever at one of it's higher transient modes, ~ 30 μT was generated. This new technique may even serve as an *alternative* B_1-source and would then replace the RF-wire or RF-coil, if at least a hundred times larger field strength could be generated. Field strengths of this order are required within common MRFM techniques such as 'oscillating cantilever adiabatic reversals' (OSCAR), as was used by Rugar for the measurement of a single electron spin [3]. This may be achieved by replacing the magnetic particle by a ferromagnet with smaller dimensions [25]. Alternatively, a combination of the relatively large NdFeB magnetic particles and a high-field nano-magnet [7] may be integrated into a new cantilever design in which the actuation of higher cantilever modes are fully exploited for high resolution MRFM data. The latter suggestion will be the subject of future study.

Appendix A

Physics of Mechanical Resonators

The computation of the dynamics of a loaded micro cantilever can be challenging and time consuming. Constrained to the geometry and parameters of the system, it is in most cases not possible to determine the analytic solution of the cantilevers equation of motion. Even the dynamics of a homogeneous 1D beam clamped at one site which is well described by the Euler-Bernoulli beam theory can only be computed numerical. A finite element analysis could be used to simulate the cantilevers motion, although the ratios of the cantilevers dimensions could result in computational errors and hence diverging solutions. Furthermore, a finite element analysis computes the time dependent displacement of all the mesh elements of the cantilever, although one is often only interested in the motion of the cantilevers tip. However, when the cantilevers oscillations are small, one can analytically approximate this tip motion by a single degree of freedom system, namely a mass-spring system where the mass is equal to the critical mass of the cantilever. The critical mass is defined as a measure of the amount of mass of the oscillator that participates within a natural oscillation mode. Below, we describe this approximation of the tip displacement.

Tip motion of a loaded cantilever at resonance

Recall the solution to the equation of motion of an unloaded mass m_{eff} attached to a spring with stiffness k:

$$\ddot{z} + \omega_0^2 z = 0 \Rightarrow z(t) = Z_0 \cos(\omega_0 t + \phi) \tag{A.1}$$

Here, $\omega_0^2 = k/m_{eff}$ is the resonance frequency of the fundamental mode and Z_0 and ϕ are determined by the initial conditions. Adding damping to the system while driving with a harmonic force complicates the equation of motion:

$$\ddot{z} + 2\delta\dot{z} + \omega_0^2 z = \frac{F_0}{m_{eff}} \cos(\Omega t) \tag{A.2}$$

where, δ is the damping factor and Ω the external drive frequency. The solution to this new 2nd order ODE is well known and is given by:

$$z(t) = z_s(t) + Z_0 \cos(\Omega t + \phi) \tag{A.3}$$

Here, $z_s(t) = A\exp(\alpha t) + B\exp(-\alpha t)$ is the solution of an underdamped system ($\delta < \omega_0$) in absence of a driving force, where A and B are determined by the initial conditions.

Furthermore, in a steady state ($t \gg 1/\delta$) the system is described by the forced oscillations and we can eliminate the 2nd term on the RHS of equation A.3, which contains all the information about the starting conditions.

Resonance occurs when $z(t)$ becomes maximal, i.e. when the external drive frequency equals Ω_R:

$$\Omega_R = \omega_0\sqrt{1 - (1/2Q^2)} \tag{A.4}$$

$$Z_{max} = \frac{2F_0Q^2}{m_{eff}\omega_0^2\sqrt{4Q^2 - 1}} \tag{A.5}$$

If this is the case we also have a phase shift $\phi = \pi/2$. For light damping ($Q \gg 1$) we see that $\Omega_R \approx \omega_0$ and A.6 reduces to:

$$Z_{max} \approx \frac{F_0Q}{k} \tag{A.6}$$

Now, if we introduce an external static force $F_{ext}(z)$ to our system, it can be shown that this force only changes the oscillator resonance frequencies and equilibrium position about which the oscillations occur. The change of these machanical properties of the resonator can be described by the following transformations:

$$\omega_0 \to \tilde{\omega_0} = \sqrt{\tilde{k}/m} \tag{A.7}$$

$$k \to \tilde{k} = k + \frac{dF_{ext}}{dz} \tag{A.8}$$

The oscillations remain similar to the previous case where there was no external force present. The new maximal displacement is now simply described by:

$$Z_{max} \approx \frac{F_0 Q}{\tilde{k}} = Q z_d \tag{A.9}$$

where z_d is the drive amplitude. For higher resonance modes, we can approximate the tip motion by assuming:

$$Z_{max}^{(n)} \approx \frac{F_0 Q_n}{\tilde{k_n}} = Q_n z_d \tag{A.10}$$

where $Z_{max}^{(n)}$, k_n and Q_n are now the tip displacement, stiffness and quality factor at the n^{th} cantilever's higher transient resonance mode respectively. Here we defined the tip displacement as the maximum height between node and anti-node. Now, the tip rotation angle θ_n can be approximated by:

$$\theta_n = \arctan\left(\frac{Z_{max}^{(n)}}{\tilde{l}_m}\right) \tag{A.11}$$

$$\tilde{l}_m = \frac{l}{2m+1} \tag{A.12}$$

where l is the cantilever length, $\tilde{l}_m$ is the reduced cantilever length and m is the number of nodes/anti-nodes of resonance mode n. For $\tilde{l}_m \ll Z_{max}^{(n)}$ equation A.11 becomes:

$$\theta_n \approx \frac{z_d Q_n}{\tilde{l}_m} \tag{A.13}$$

Bibliography

[1] J. A. Sidles, *Noninductive detection of single-proton magnetic resonance*, Applied Physics Letters **58**, 2854 (1991).

[2] J. A. Sidles, *Folded Stern-Gerlach experiment as a means for detecting nuclear magnetic resonance in individual nuclei*, Physical Review Letters **68**, 1124 (1992).

[3] D. Rugar, R. Budakian, H. J. Mamin, and B. W. Chui, *Single spin detection by magnetic resonance force microscopy.*, Nature **430**, 329 (2004).

[4] C. L. Degen, M. Poggio, H. J. Mamin, C. T. Rettner, and D. Rugar, *Nanoscale magnetic resonance imaging*, P. Natl. Acad. Sci. **106**, 1313 (2009).

[5] F. Bloch, *Dynamical theory of nuclear induction. II*, Physical Review **102**, 104 (1956).

[6] M. de Voogd, J. Wagenaar, and T. H. Oosterkamp, *Dissipation and resonance frequency shift of a resonator magnetically coupled to a semiclassical spin*, arXiv:1508.07972v1 (2015).

[7] J. G. Longenecker, H. Mamin, A. W. Senke, L. Chen, C. T. Rettner, D. Rugar, and J. Marohn, *High-Gradient Nanomagnets on Cantilevers for Sensitive Detection of Nuclear Magnetic Resonance*, ACS Nano , 9637 (2012).

[8] A. Vinante, L. Schinkelshoek, O. Usenko, G. Wijts, and T. H. Oosterkamp, *Magnetic Resonance Force Microscopy of paramagnetic electron spins at millikelvin temperatures*, Nature Communications **2**, 6 (2011).

[9] F. Pobell, *Matter and Methods at Low Temperatures*, 3 edition, 2007.

[10] G. Wijts, *Magnetic Resonance Force Microscopy at milliKelvin Temperatures*, PhD thesis, 2013.

[11] A. M. J. Den Haan, *Nuclear magnetic resonance at millikelvin temperatures*, PhD thesis, 2016.

[12] B. W. Chui, Y. Hishinuma, R. Budakian, H. J. Mamin, T. W. Kenny, and D. Rugar, *Mass-loaded cantilevers with suppressed higher-order modes for magnetic resonance force microscopy*, TRANSDUCERS, Solid-State Sensors, Actuators and Microsystems, 12th International Conference on, 2003 **2**, 1120 (2003).

[13] A. M. J. Den Haan, J. J. T. Wagenaar, J. M. De Voogd, G. Koning, and T. H. Oosterkamp, *Spin-mediated dissipation and frequency shifts of a cantilever at milliKelvin temperatures*, Physical Review B - Condensed Matter and Materials Physics **92**, 1 (2015).

[14] A. Vinante, A. Kirste, A. Den Haan, O. Usenko, G. Wijts, E. Jeffrey, P. Sonin, D. Bouwmeester, and T. H. Oosterkamp, *High sensitivity SQUID-detection and feedback-cooling of an ultrasoft microcantilever*, Applied Physics Letters **101** (2012).

[15] J. J. T. Wagenaar, A. M. J. den Haan, J. M. de Voogd, T. A. de Jong, M. de Wit, K. M. Bastiaans, D. J. Thoen, A. Endo, T. M. Klapwijk, J. Zaanen, and T. H. Oosterkamp, *Supplemental Material for 'Probing the nuclear spin-lattice relaxation time at the nanoscale'*, ArXiv , 1 (2016).

[16] A. M. J. Den Haan, J. J. T. Wagenaar, and T. H. Oosterkamp, *Magnetic resonance with amplification of B 1 by cantilever displacement (ABCD) at millikelvin temperatures*, page 1 (2016).

[17] G. Duffing, *Erzwungene Schwingungen bei Veränderlicher Eigenfrequenz*, F. Vieweg U. Sohn, Braunschweig, 1918.

[18] J. Kawamura, J. Chen, D. Miller, J. Kooi, and J. Zmuidzinas, *Low-noise submillimeter-wave NbTiN superconducting tunnel junction mixers*, Appl. Phys. Lett. **75**, 4013 (1999).

[19] K. M. Bastiaans, *Power dissipation of a type II superconducting microwire carrying large oscillating currents at low temperatures*, PhD thesis, Leiden University, 2015.

[20] J. Wagenaar, A. M. J. den Haan, J. de Voogd, T. de Jong, M. de Wit, K. Bastiaans, D. Thoen, A. Endo, T. Klapwijk, J. Zaanen, and T. Oosterkamp, *Probing the nuclear spin-lattic relaxation time at the nanoscale*, ArXiv:1603.04238 (2016).

[21] I. Rabi, N. Ramsey, and J. Schwinger, *Use of rotating coordinates in Magnetic Resonance Problems*, Reviews of Modern Physics **26** (1954).

[22] A. S. Oja and O. V. Lounasmaa, *Nuclear magnetic ordering in simple metals at positive and negative nanokelvin temperatures*, Reviews of Modern Physics **69**, 1 (1997).

[23] M. T. Huiku, T. A. Jyrkki, J. M. Kyyniiriiinen, and M. T. Loponen, *Investigations of Nuclear Antiferromagnetic Ordering in Copper at Nanokelvin Temperatures*, **62**, 433 (1986).

[24] G. P. Berman, V. N. Gorshkov, D. Rugar, and V. I. Tsifrinovich, *Spin Relaxation Caused by Thermal Excitations of High Frequency Modes of Cantilever Vibrations*, Physical Review B - Condensed Matter and Materials Physics **68**, 094402 (2003).

[25] H. C. Overweg, A. M. J. den Haan, H. J. Eerkens, P. F. A. Alkemade, A. L. La Rooij, R. J. C. Spreeuw, L. Bossoni, and T. H. Oosterkamp, *Probing the magnetic moment*

of FePt micromagnets prepared by focused ion beam milling, Applied Physics Letters **107**, 072402 (2015).

Acknowledgements

When I arrived at the Leiden nano-MRI group, I was fortunate to be the very first student that could work with an operational set-up, a privilege that is everything but evident within cutting edge research. Although I did not had the honour to meet all of them in person, I would like to express my deep gratitude to everyone who was involved in the development of our MRFM apparatus.

The results as reported in this thesis are built on the foundation as provided by many persons: All my present and former colleagues at the nano-MRI group, including all supporting academic staff at the Fine Mechanics Department, the Leiden Electronic Department and Leiden Cryogenics.

I would like especially to offer my thanks to Jelmer Wagenaar for his guidance and support. Jelmer, as appeared to me as a very skilled researcher and an excellent teacher, was the architect of most experiments that I performed during my stay. I am grateful that he shared his knowledge and expertise with me.

Moreover, I would like to thank my supervisor, Tjerk Oosterkamp, for his advise and trust. He gave me the opportunity to witness the development of a very promising field, an experience that gave me new energy, inspiration and passion for physics. It was a real pleasure to be part of his group.